CHIMERA MICROSCOPIC APPROACH TO HEAVY ION COLLISIONS AT INTERMEDIATE ENERGIES*

J. ŁUKASIK AND Z. MAJKA

Institute of Physics, Jagellonian University
PL-30-059 Kraków, Reymonta 4, Poland

(Received April 29, 1993)

A microscopic model based on a molecular dynamics concept is presented. The model simulates some quantum effects and thus enables studies of large fermionic systems. It was devised to investigate the dynamics of heavy ion collisions at intermediate energies. The model was applied to study an early phase of the $^{84}Kr+^{159}Tb$ reaction at 45 MeV/nucleon.

PACS numbers: 24.10. Cn, 25.70. -z

1. Introduction

The study of nuclear matter in equilibrium has progressed a lot. For instance, the equation of state (EOS) is not completely unknown to us if one stays near saturation point $\rho = \rho_0$ (normal nuclear density $\rho = 0.17$ fm^{-3}) and temperature $T = 0$. Other regions in the ρ and T plane are more uncertain, and the past decade has seen a vigorous growth of activity (both in experiment and theory) to obtain information about the nuclear EOS and strong interaction vertices at high nuclear densities. Theoretical calculations predict that (ρ, T) plane is full of structure [1]. However, this is very difficult to investigate in a laboratory where only normal stable nuclei are available and energetic heavy ion collisions encounter a lot of problems. First of all, in a laboratory the maximum size of nuclear system around 500 nucleons can be formed from colliding two of the largest nuclei. Moreover, collision between nuclei usually produces a lot of excess heat and this prevents us from reaching certain parts of the phase space.

* The work was supported by the Scientific Research Committee under Grant No. 2 2392 91 02.

Another problem is that the life time of the colliding system is very short and we deal with a non-equilibrium states. How can we conclude anything from the above concerning a microscopic equilibrium property like the EOS? The best we can do is to observe the non-equilibrium phenomena and infer its consequences for equilibrium situation. Therefore, we need a realistic description of heavy ion collisions through a dynamical approach and compare its results with experimental data. The main trend in experiments is to go from inclusive to more exclusive measurements. This allows to discriminate between phenomenological models based on very different approximations. The progress is made also in the theory where advanced microscopic models are proposed.

Nucleus–nucleus collisions at a few MeV per nucleon above the interaction barrier are governed by mean field potential. At these energies the Pauli principle forbids nucleon–nucleon collisions into already occupied states and due to long mean-free-path of the nucleons they can be viewed as moving in self consistent potential. The time dependent Hartree–Fock model successfully describes dynamics of collision between heavy ions in this low energy domain [2].

If the beam energy is about 200 MeV/nucleon or more, the nuclear binding energy can be neglected and only the two body nucleon - nucleon dynamics is represented in the intra nuclear cascade model developed for high energy heavy ion collision [3].

The important feature which emerged from the study of heavy ion collision is that the equilibrium states can be found in both very low and very high energy regions. In between these two extremes is intermediate energy heavy ion physics which concerns projectile with incident energy from 20 to 200 MeV/nucleon. Here, the mean field (one body) and nucleon–nucleon (two body) dynamics are of comparable importance and equilibration of the system is questionable. Moreover, two novel phenomena were observed, namely, multifragmentation [4] and collective flow of nuclear matter [5]. The observation that two colliding ions do not equilibrate in course of the reaction implies a tremendous complication of the problem. Here we have to trace the details of the dynamics from the initial state of colliding ions up to the final distribution of reaction products in phase space. The time evolution of two colliding nuclei in phase space has been first calculated successfully in hydrodynamical approach [6]. Currently, the theoretical framework which contains both the mean field and hard collisions is based on Boltzmann–Uehling–Uhlenbeck equation [7]. The predictions of this model are limited to one-body observables (the equation describes the evolution of one body distributions). Here we present a semiclassical model developed for simulation of nuclear reactions between heavy ions at intermediate energy. Our approach is based on the quantum molecular

dynamics model [8–10, 21] and the quasi-particle model [11, 12]. The simulations performed allow one to follow the time evolution of positions and momenta of the individual nucleons. The model Hamiltonian apart from the Coulomb and isospin-dependent terms incorporates the antisymmetrization effects through a momentum dependent potential. The colliding nuclei have a well-defined ground state with non-vanishing expectation value of the kinetic energy operator. The layout of the report is as follows. In Section 2 we present the description of the model. Section 3 contains some of the model predictions.

2. Model

2.1. General assumptions

The model, or rather its numerical implementation dubbed CHIMERA (Code for Heavy Ion Medium Energy ReActions), presented in this paper is a compilation of two recently devised models which utilize the molecular dynamics[1] concept to describe the bulk properties of the intermediate (20-200 MeV/nucleon) energy nuclear reactions. These are the Quantum Molecular Dynamics (QMD) model of Aichelin and Stöcker [8–10, 21] and the Quasi-Particle Dynamics (QPD) model of Boal and Glosli [11, 12]. In principle these two models are very similar. The main difference between them is the way of preparing the initial configurations and the N-N potentials used.

In order to investigate the time evolution of the heavy ion collisions one has to find reasonable approximations to the time dependent N-body Schrödinger equation. One of the ways of such an approximate solution present the above mentioned models. A thorough theoretical background of the QMD model including the derivation of the QMD equation and the necessary approximations are presented in a review article of Jörg Aichelin [10]. Here we list only the main assumptions that apply also to the CHIMERA code:

- the scattering of the nucleons can be treated as if they were free (stochastic scattering with the measured nucleon–nucleon cross section);
- the collisions are statistically independent and the interference between two different collisions can be neglected;
- the real part of the transition matrix can be replaced by an effective potential;
- the fermionic nature of the nucleons can be mimicked without an explicit use of the antisymmetrized wave functions.

---

[1] The molecular dynamics models use the equation of motion approach to solving the many body problems. They have their roots in chemistry.

For discussion of validity of these assumptions the reader is referred to the Ref. [10].

The approximate solution of the quantal N-body problem in the QMD approach requires the initial N-body wave function (or equivalently the Wigner representation of the respective density matrix) as input. In the model described in this paper, each nucleon (or quasi-particle) is assumed to be a constant width minimal wave packet (coherent state):

$$\psi_i(\vec{r},t) = \frac{1}{(2\pi L)^{3/4}} \exp\left(-\frac{(\vec{r}-\vec{r}_{0i}(t))^2}{4L}\right) \exp\left(-\frac{i}{\hbar}\vec{p}_{0i}(t)\vec{r}\right), \qquad (1)$$

where $\vec{r}_{0i}$ and $\vec{p}_{0i}$ are the mean position and momentum of the nucleon i and the width of the wave packet is characterized by the parameter L. The Gaussian form was adopted for the single particle wave function for at least three reasons. First of all, the minimal wave packet (m.w.p.) fulfills the minimal requirement of the uncertainty principle:

$$\Delta r_x \Delta p_x = \frac{\hbar}{2}.$$

Secondly, the one body density distribution constructed from this packets coincides with the observed density profiles. And last but not least, the Gaussian wave packets make the calculations feasible. The width of the wave packet is kept constant contrary to the solution of a free Shrödinger equation which spreads in time. Keeping L constant is in agreement with the observation that the radius of a cold nucleus is stationary and thus imitates in a crude way the influence of the potential on the wave function.

The N-body "wave function", ψ_N, describing the entire nucleus is taken to be a direct product of N single particle states ψ_i. This, of course, is a violation of the antisymmetry rules. Here it is assumed that the fermionic effects, which are believed to be essential for the reasonable treatment of the dynamics, can be simulated with the use of an effective potential term (Pauli potential) and with Pauli blocking of final states of individual N-N collisions. The Pauli potential plays an important role during initialization of a cold nucleus. It prevents the nucleons of the same kind from being too close in phase space.

The quantum mechanical analogue of a classical N-body phase space density distribution function is a Wigner transform of the density matrix

[13]. In the case of m.w.p. (Eq. (1)) this reads:

$$
\begin{aligned}
f^{(N)}&(\vec{R}_1,\vec{R}_2,\ldots,\vec{R}_N,\vec{p}_1,\vec{p}_2,\ldots,\vec{p}_N) \\
&\equiv \frac{1}{(2\pi\hbar)^{3N}}\int\left(\prod_{i=1}^{N}d^3r_i\right)\exp\left(-\frac{i}{\hbar}\sum_{k=1}^{N}\vec{p}_k\vec{r}_k\right) \\
&\times\psi_N^*\left(\vec{R}_1-\frac{\vec{r}_1}{2},\ldots,\vec{R}_N-\frac{\vec{r}_N}{2}\right)\psi_N\left(\vec{R}_1+\frac{\vec{r}_1}{2},\ldots,\vec{R}_N+\frac{\vec{r}_N}{2}\right) \\
&=\frac{1}{(\pi\hbar)^{3N}}\exp\left(-\frac{1}{2L}\sum_{k=1}^{N}(\vec{R}_k-\vec{r}_{0k})^2-\frac{2L}{\hbar^2}\sum_{k=1}^{N}(\vec{p}_k-\vec{p}_{0k})^2\right).
\end{aligned}
$$

In the present approach we restrict ourselves to the single particle reduced distribution function [14]:

$$
\begin{aligned}
f(\vec{r},\vec{p}) &\equiv \int\left(\prod_{k=1}^{N}d^3R_kd^3p_k\right) \\
&\times\sum_{i=1}^{N}\delta(\vec{r}-\vec{R}_i)\delta(\vec{p}-\vec{p}_i)f^{(N)}(\vec{R}_1,\vec{R}_2,\ldots,\vec{R}_N,\vec{p}_1,\vec{p}_2,\ldots,\vec{p}_N) \\
&=\frac{1}{(\pi\hbar)^3}\sum_{i=1}^{N}\exp\left(-\frac{1}{2L}(\vec{r}-\vec{r}_{0i})^2\right)\exp\left(-\frac{2L}{\hbar^2}(\vec{p}-\vec{p}_{0i})^2\right)
\end{aligned}
$$

which describes the single particle density of phase space in the point $(\vec{r},\vec{p})$. The one-body densities in coordinate and momentum space are now:

$$
\rho(\vec{r})=\int f(\vec{r},\vec{p})d^3p=\frac{1}{(2\pi L)^{3/2}}\sum_{i=1}^{N}\exp\left(-\frac{1}{2L}(\vec{r}-\vec{r}_{0i})^2\right), \tag{2}
$$

$$
g(\vec{p})=\int f(\vec{r},\vec{p})d^3r=\left(\frac{2L}{\pi\hbar^2}\right)^{3/2}\sum_{i=1}^{N}\exp\left(-\frac{2L}{\hbar^2}(\vec{p}-\vec{p}_{0i})^2\right). \tag{3}
$$

The time evolution of the N-body "wave function" describing the entire system is assumed to be governed by the Ritz variational principle [10, 15]. In fact it reduces to the classical Hamilton equations of motion for the centroids of the Gaussian wave packets. Thus the mean positions and momenta of N nucleons are assumed to evolve due to mutual two and three body effective N-N interactions along classical trajectory in phase space.

The influence of the scattering term on the time evolution of the system is simulated by a Monte Carlo procedure. Whenever two nucleons come closer than the distance determined by a free N-N cross section, they are assumed to scatter isotropically, provided the final states are not blocked. Only the elastic channel of the N-N scattering is assumed — no gamma or particle production is implemented. This, together with the fact that the nonrelativistic kinematics is used, sets the upper limit of the incident energies for CHIMERA to about 150 MeV/nucleon.

Such rough approximations seem to be the only reasonable way to handle the dynamics of N-body nuclear systems (N up to 500), with the use of the present day computers.

2.2. Effective nucleon–nucleon potential

Combining the local density approximation (see *e.g.* [16]) with the assumption that the real part of the transition matrix can be replaced by an effective potential, one can adopt the nuclear matter effective interactions to finite nuclear objects. Following Boal [11] we use the nuclear effective potential derived from the Skyrme parametrization of the nuclear potential energy density V_N:

$$V_N = \frac{\alpha}{2}\frac{\rho^2}{\rho_0} + \frac{\beta}{\gamma+1}\frac{\rho^{\gamma+1}}{\rho_0^{\gamma}} + \frac{\omega}{2}\frac{(\rho_p-\rho_n)^2}{\rho_0} + \frac{G}{2}(\nabla\rho)^2, \tag{4}$$

where the term with the gradient of the density accounts for the surface effects, ρ_p and ρ_n are the proton and neutron densities, and ρ_0 is the normal nuclear matter density ($\rho_0 = 0.17$ fm^{-3}). Introduction of γ instead of a constant exponent equal to 3 allows for generalization of the EOS for various compressibilities.

For m.w.p. the nuclear potential energy approximately reads:

$$\begin{aligned} U_N &= \int V_N d^3r \\ &\simeq \frac{\alpha}{2\rho_0}\sum_{i=1}^{N}\sum_{\substack{k=1\\k\neq i}}^{N}\tilde{\rho}_{ik} + \frac{\beta}{(\gamma+1)\rho_0^{\gamma}}\sum_{i=1}^{N}\Big(\sum_{\substack{k=1\\k\neq i}}^{N}\tilde{\rho}_{ik}\Big)^{\gamma} \\ &\quad + \frac{\omega}{2\rho_0}\sum_{i=1}^{N}\sum_{\substack{k=1\\k\neq i}}^{N}\xi_i\xi_k\tilde{\rho}_{ik} + \frac{G}{8L^2}\sum_{i=1}^{N}\sum_{\substack{k=1\\k\neq i}}^{N}(6L - r_{ik}^2)\tilde{\rho}_{ik}, \end{aligned} \tag{5}$$

where: $\vec{r}_{ik} = \vec{r}_{0i} - \vec{r}_{0k}$, $\xi_i = \begin{cases} +1 & \text{for protons} \\ -1 & \text{for neutrons} \end{cases}$, and the "interaction density" $\tilde{\rho}_{ik} = \Big(1/(4\pi L)^{3/2}\Big)\exp\big(-(1/4L)(\vec{r}_{0i} - \vec{r}_{0k})^2\big)$.

The nuclear potential is supplemented by the momentum dependent Pauli potential and the Coulomb potential.

The Pauli potential was devised in order to simulate the antisymmetrization effects. There were several phenomenological approaches to derive the form of this potential (see *e.g.* Wilets [17], Dorso and Randrup [18], Horiuchi [19]), but the most reliable seems to be the derivation proposed by Boal and Glosli [11]. They considered the influence of antisymmetrization on the total kinetic energy of a nucleon pair. The expectation value of the kinetic energy of two like nucleons is:

$$\begin{aligned}\langle K\rangle &\equiv -\frac{\hbar^2}{2m}\langle\psi^{(2)}(\vec{r}_i,\vec{r}_j)|\nabla_i^2+\nabla_j^2|\psi^{(2)}(\vec{r}_i,\vec{r}_j)\rangle \\ &= \frac{1}{2m}\left[p_{0i}^2+p_{0j}^2+\frac{3\hbar^2}{2L}+\frac{\hbar^2}{8L^2}\frac{Q_{ij}^2}{e^{\frac{1}{4L}Q_{ij}^2}-1}\right]. \qquad (6)\end{aligned}$$

where $\psi^{(2)}$ is an antisymmetrized two body wave function in the m.w.p. representation and Q_{ij}^2 is a measure of the distance in phase space:

$$Q_{ij}^2=(\vec{r}_{0i}-\vec{r}_{0j})^2+\frac{4L^2}{\hbar^2}(\vec{p}_{0i}-\vec{p}_{0j})^2. \qquad (7)$$

The third term in expression (6) follows from the finite width of the wave packet and has no dynamical consequences. The last term is a result of the antisymmetrization and is identified as a Pauli potential. Thus the total energy arising from the "Pauli interaction" reads:

$$U_P=\frac{1}{2}V_0^P\frac{\hbar^2}{16mL^2}\sum_{i=1}^{N}\sum_{\substack{j=1\\ j\neq i}}^{N}\frac{Q_{ij}^2}{\exp\left(\frac{1}{4L}Q_{ij}^2\right)-1}\delta_{t_it_j}\delta_{s_is_j}. \qquad (8)$$

Where the Kronecker deltas ensure that the potential acts between like quasi-particles only. The scale factor $V_0^P>1$ was introduced in order to reproduce the energetics of three- and higher-body systems. Its value was found to be between 1.7 and 1.9 [11].

The Coulomb potential for Gaussian charge distribution can be expressed in terms of the error functions:

$$^{\text{Gauss}}V_C^{ij}=\frac{e^2}{r_{ij}}\operatorname{erf}\left(\frac{r_{ij}}{2\sqrt{L}}\right). \qquad (9)$$

It is very convenient to introduce the approximation of sharp charged spheres instead of Gaussian distributions. V_C^{ij} then simplifies to:

$$^{\text{sphere}}V_C^{ij}=\begin{cases}\frac{e^2}{r_{ij}} & r_{ij}>r_{0c}\\ \frac{e^2\left(3-(r_{ij}/r_{0c})^2\right)}{2r_{0c}} & r_{ij}\leq r_{0c}\end{cases}, \qquad (10)$$

where: $r_{0c} = {}^3/_2\sqrt{\pi L}$ and $r_{ij} = |\vec{r}_{0i} - \vec{r}_{0j}|$.

The total Coulomb energy of the system now reads:

$$U_C = \tfrac{1}{2}e^2 \sum_{i=1}^{N} \sum_{\substack{j=1 \\ j\neq i}}^{N} {}^{\text{sphere}}V_C^{ij} \, (\tfrac{1}{2} + t_{3i})(\tfrac{1}{2} + t_{3j}) \,, \tag{11}$$

where the last two factors exclude neutrons from the summation.

Now the total N-body Hamiltonian has the form:

$$H = \sum_{i=1}^{N} \frac{p_{0i}^2}{2m} + U_N + U_P + U_C \,. \tag{12}$$

2.3. Parameter values

There are seven parameters in the potential formula. These are the width of the wave packet L, the Pauli potential scale factor V_0^P and five nuclear potential parameters: α, β, γ, ω and G.

The first approximation for the parameters α, β and γ can be made using the parameters of the infinite nuclear matter potential, U^{loc}, in the Skyrme parametrization:

$$U^{\text{loc}} = \alpha \left(\frac{\rho}{\rho_0}\right) + \beta \left(\frac{\rho}{\rho_0}\right)^{\gamma} .$$

For the hard EOS (nuclear matter compressibility $K = 380$ MeV) these parameters have the following values [9]:

$$\alpha = -124 \text{ MeV}, \quad \beta = 70.5 \text{ MeV}, \quad \gamma = 2 \,.$$

For the calculational purposes we adopt all the values found by Boal [11] (with a slight modification of the α parameter). These values were found to give the best possible values of binding energies and rms radii of the beta stable nuclei with A from 2 to 200. The procedure of finding the ground state configurations as well as the ground state properties of the model nuclei will be presented in the next section.

The values of the potential parameters for the hard EOS used in the CHIMERA code are listed in the Table I. The soft EOS will be the subject of the separate paper.

TABLE I

Parameters of the potential

L [fm^2]	α [MeV]	β [MeV]	γ	ω [MeV]	G [MeV fm^5]	V_0^P
2.0	-124.69	74.24	2.0	30.54	291.0	1.9

2.4. Ground state configurations

The ground state configuration (g.s.c.) is the configuration in phase space that minimizes the Hamiltonian H of the system. Mathematically the problem of finding the g.s.c. reduces to solving a set of $6N$ nonlinear equations:

$$\begin{cases} \frac{\partial H}{\partial \vec{r}_{0i}} = 0 \\ \frac{\partial H}{\partial \vec{p}_{0i}} = 0 \,. \end{cases} \tag{13}$$

This numerically complicated task may be solved with the help of physics. Namely one can utilize the fact that the physical system, when allowed to dissipate its energy, reaches its g.s.c. after sufficiently long time. This may be expressed in the form of the dumped equations of motion [11, 17]:

$$\begin{cases} \dot{\vec{r}}_{0i} = \frac{\partial H}{\partial \vec{p}_{0i}} - \frac{u}{v} \frac{\partial H}{\partial \vec{r}_{0i}} \\ \dot{\vec{p}}_{0i} = -\frac{\partial H}{\partial \vec{r}_{0i}} - u \frac{\partial H}{\partial \vec{p}_{0i}} \,. \end{cases} \tag{14}$$

We found that the values of $u = 180$ MeV/fm c and $v = 1000$ (MeV/fm c)^2 ensure fast convergent cooling process along the smoothest cooling curve (binding energy vs temperature). After 200 fm/c the initially hot nuclei are cooled down to $T \simeq 0$ almost independently of the starting configuration of the nucleons.

There are also other methods of cooling the excited nuclei reported in the literature. These are the methods based on the Metropolis sampling technique [20, 18, 21] and the collisional cooling method of Refs [19, 22].

The ground state binding energies and rms radii of the model nuclei are presented in Fig. 1. The binding energies are compared to the experimental values taken from the Wapstra tables. The line labelled "Fermi" in the lower part of Fig. 1 presents the best fit to the experimental root mean square radii, assuming the Fermi distribution of the nuclear density. As can be seen the model reproduces very well the bulk static properties of heavy nuclei for which the local density approximation is the best.

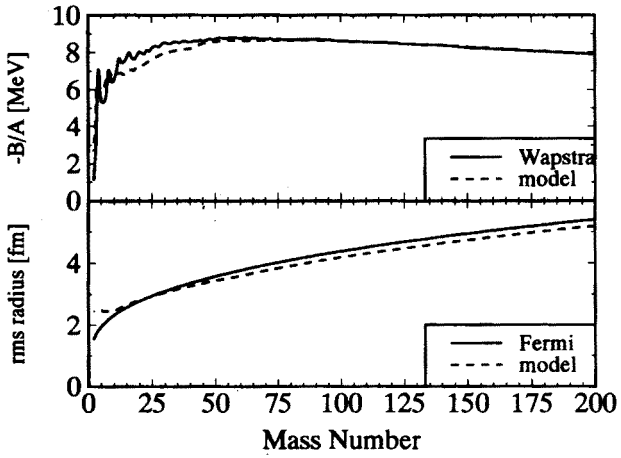

Fig. 1. Binding energies and rms radii of the model nuclei.

2.5. Initial conditions of nuclear collision

The cooled nuclei are now used in the investigation of the dynamics of nuclear collisions. Two colliding ions are assumed to move along classical Coulomb trajectories until the distance between their surfaces is 3 fm (see Fig. 2). This distance was found to be the best compromise between the

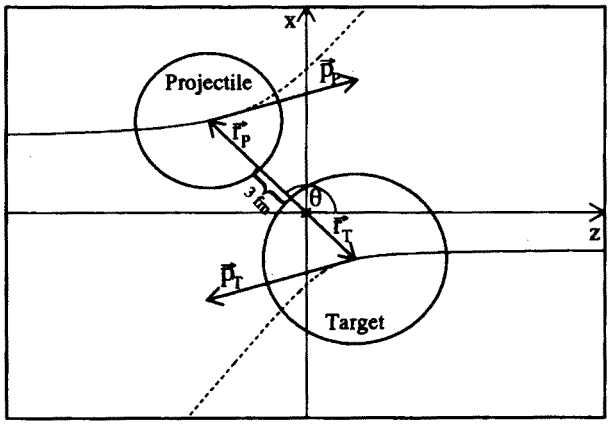

Fig. 2. Initial positions and momenta of colliding ions.

consequence of neglecting of the nuclear force at such a separation, and the requirement to save as much computer time as possible. The positions and momenta presented in Fig. 2 are treated as a starting point for further $A_P + A_T$ body dynamics. These initial positions of centers of mass $(\vec{r}_P, \vec{r}_T)$

and linear momenta $(\vec{p}_P, \vec{p}_T)$ of the colliding ions in their CM reference frame are uniquely determined by the initial projectile LAB energy E_0 and the impact parameter b:

$$\begin{cases} \vec{r}_P = \frac{\mu}{m_P}\vec{r} \\ \vec{r}_T = -\frac{\mu}{m_T}\vec{r} \end{cases} \qquad \begin{cases} \vec{p}_P = m_P \dot{\vec{r}}_P \\ \vec{p}_T = m_T \dot{\vec{r}}_T \end{cases},$$

where:

$$\vec{r} = r(\sin\theta, 0, \cos\theta), \quad r = R_P + R_T + 3\,\text{fm},$$

$$\theta = \pi + \arccos\left(\frac{\frac{p}{r}+1}{\varepsilon}\right) - \arccos\left(\frac{1}{\varepsilon}\right),$$

$$p = \frac{2\mu b^2 E_0}{m_P \zeta}, \quad \varepsilon = \sqrt{\frac{p^2}{b^2}+1},$$

$$\zeta = Z_P Z_T e^2, \quad \mu = \frac{m_P\, m_T}{m_P + m_T},$$

the indices P and T refer to projectile and target, and m, μ, R, Z and e stand for the mass of the ion, the reduced mass of the system, the radius and the atomic number of the ion and the elementary electric charge, respectively.

The centers of projectile and target ions are now placed in the $\vec{r}_P$ and $\vec{r}_T$ positions and a respective collective component of the linear momentum per nucleon $\vec{p}_P/A_P$ or $\vec{p}_T/A_T$ is added to the linear momentum of each nucleon.

The cooling procedure is rather time consuming, so in order to increase the efficiency of calculations once cooled nucleus is used in several subsequent collisions after rotation about random Euler angles.

Having defined the initial conditions for the set of $6(A_P + A_T)$ equations of motion of nucleons, one can proceed to solving this set.

2.6. Time evolution of the system

The time evolution of the centroids of the Gaussian wave packets is described by two processes: the propagation due to classical equation of motion and the stochastic short range two body scattering. The equations of motion:

$$\begin{cases} \dot{\vec{r}}_{0i} = \frac{\vec{p}_{0i}}{m} + \vec{\nabla}_{p_{0i}} U \\ \dot{\vec{p}}_{0i} = -\vec{\nabla}_{r_{0i}} U \end{cases} \qquad i = 1, \ldots, A_P + A_T\,, \tag{15}$$

are solved numerically with the use of the two step Euler method with a constant time step. In the first step (Eq. (16)) the positions and momenta are determined with the use of the ordinary Euler method in the middle of the time step. In the second step (Eq. (17)) the previously determined positions and momenta are used to calculate the gradients of the potential, and these values are used to calculate the new positions and momenta at

the end of the time step. This procedure ensures the accuracy of the second order method. Thus for the n-th time step we have:

$$(I)\quad \begin{cases} \vec{r}_{0i}(n+\frac{1}{2}) = \vec{r}_{0i}(n) + \frac{\Delta t}{2}\left(\frac{\vec{p}_{0i}(n)}{m} + \vec{\nabla}_{p_{0i}} U(n)\right) \\ \vec{p}_{0i}(n+\frac{1}{2}) = \vec{p}_{0i}(n) - \frac{\Delta t}{2}\vec{\nabla}_{r_{0i}} U(n)\,, \end{cases} \tag{16}$$

$$(II)\quad \begin{cases} \vec{r}_{0i}(n+1) = \vec{r}_{0i}(n) + \Delta t\left(\frac{\vec{p}_{0i}(n+\frac{1}{2})}{m} + \vec{\nabla}_{p_{0i}} U(n+\frac{1}{2})\right) \\ \vec{p}_{0i}(n+1) = \vec{p}_{0i}(n) - \Delta t\vec{\nabla}_{r_{0i}} U(n+\frac{1}{2})\,. \end{cases} \tag{17}$$

A search is made in each time step if there are any candidates for the collision in the system. Any two nucleons become candidates for scattering if their spatial distance is less than the distance determined by the free N-N cross section (see *e.g.* Bertch and Das Gupta [23]):

$$r_{ij} < \sqrt{\frac{\sigma_{NN}}{\pi}}\,,$$

Now the possible new momenta are determined assuming isotropic scattering. The collision is allowed if the new states are not already occupied by the like nucleons. Otherwise the collision is blocked and the two nucleons continue their movement in the effective potential. Thus the scattering probability is proportional to the effective (*i.e.* Pauli corrected) N-N cross section. Following Aichelin [8] we use the value of 41 mb for the free σ_{NN}. The assumption of the isotropic (*i.e.* S wave) scattering causes some inaccuracy in the angular momentum conservation. Thus the angular momentum is conserved only "statistically". This is the price for the assumption of the stochastic character of the scattering (*i.e.* the assumption of no relation between the impact parameter and the scattering angle) following from the probabilistic interpretation of the cross section.

The total energy and linear momentum of the system can not be altered by the elastic stochastic scattering. This leads to the following conditions for any two nucleons changing their linear momenta from $(\vec{p}_{01}, \vec{p}_{02})$ to $(\vec{p}_{01'}, \vec{p}_{02'})$:

$$\begin{cases} \vec{p}_{01} + \vec{p}_{02} = \vec{p}_{01'} + \vec{p}_{02'} \\ \frac{p_{01}^2 + p_{02}^2}{2m} + U_P(\vec{p}_{01}, \vec{p}_{02}, \ldots, \vec{p}_{0N}) = \frac{p_{01'}^2 + p_{02'}^2}{2m} + U_P(\vec{p}_{01'}, \vec{p}_{02'}, \ldots, \vec{p}_{0N})\,, \end{cases} \tag{18}$$

where the "primed" indices refer to the post scattering state. The presence of the momentum dependent Pauli potential complicates the solution of the set (18). It has to be done numerically.

Every time the two nucleons become candidates for the stochastic scattering, the phase space around their final states is checked. The occupancy of phase space $\chi_{01'}$ around the 1'-st scattered nucleon is assumed to be the overlap of the phase space distribution of the 1'-st nucleon with the phase space distributions of all the remaining nucleons i but the 1-st one:

$$\chi_{01'} = \sum_{i \neq 1} \mathrm{erfc}\left(\frac{Q_{1'i}}{2\sqrt{2L}}\right), \tag{19}$$

where the Q_{ji} is a measure of the distance in phase space defined in equation (7). Now the occupancy is compared to a random number ξ. If $\xi < \chi_{01'}$ then the collision is blocked, otherwise the whole procedure is repeated for the second scattered nucleon 2'. If the phase space around the 2' nucleon turns out to be essentially free then the new positions and momenta 1' and 2' are accepted, otherwise the collision is blocked.

2.7. Characteristics of the reaction products

After a specified time the dynamical evolution is stopped. Now a cluster search routine is called. All nucleons which are separated in the configuration space by less then 3 fm are said to form a cluster. Each cluster has then assigned a mass number, atomic number, CM position, linear momentum, binding energy, temperature and spin. The binding energy allows for later determination of the excitation energy. The temperature of the cluster ν is defined as (see *e.g.* Huang [24]):

$$T_\nu = \frac{1}{3A_\nu} \sum_{i \in \{\nu\}} \vec{p}_{0i} \frac{\partial H}{\partial \vec{p}_{0i}}, \tag{20}$$

where A_ν is the mass number of the cluster ν.

3. Model predictions

In this section we present a systematic survey of the calculated characteristics currently used to describe the time evolution of the reaction between heavy ions. We applied the model to simulate the reaction 45 MeV/nucleon ^{84}Kr+^{159}Tb, which has been investigated experimentally [25].

In order to develop an intuitive picture for the reaction scenario, we show in Fig. 3 the coordinate space positions of the nucleons in a single collision at seven time intervals and for four impact parameters. The time, $t = 0$ fm/c, corresponds to the configuration when the surfaces of the projectile and target nuclei are separated by 3 fm. In the central collision a

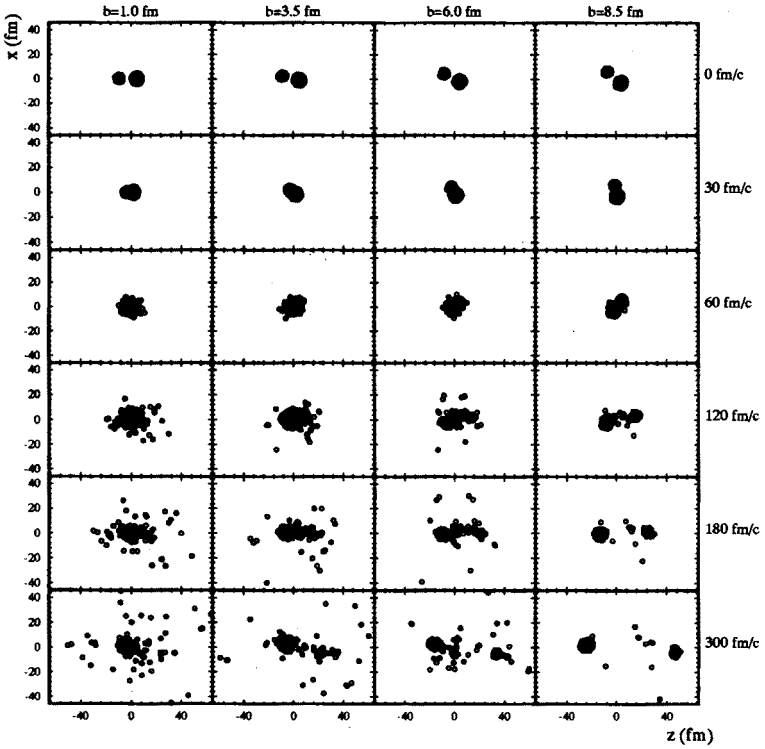

Fig. 3. The time evolution of the system for various impact parameters.

fused system is formed and for larger impact parameters the binary character of the reaction is observed. The number of the emitted nucleons and fragments decreases for less violent collisions.

To determine the time evolution of the reaction in a more quantitative way, the following procedure was applied. During each event of the simulation, the positions and momenta of each nucleon were stored at selected time steps. By tracing back through the stored values and averaging over many events, one could determine the time evolution of several quantities.

In Fig. 4(a) we show the time evolution of the mean density of the whole system, defined as a mean value of the density ρ from Eq. (2):

$$\langle \rho \rangle = \frac{\int \rho^2(\vec{r}) d^3r}{\int \rho(\vec{r}) d^3r} . \tag{21}$$

Fig. 4(b) displays the total emission rates of the neutrons, light charged particles ($Z \leq 2$), LCP, and intermediate mass fragments ($3 \leq Z \leq 20$), IMF. Both quantities were calculated at various impact parameters between 0 and 10 fm. First, it can be seen that the time evolution of the average

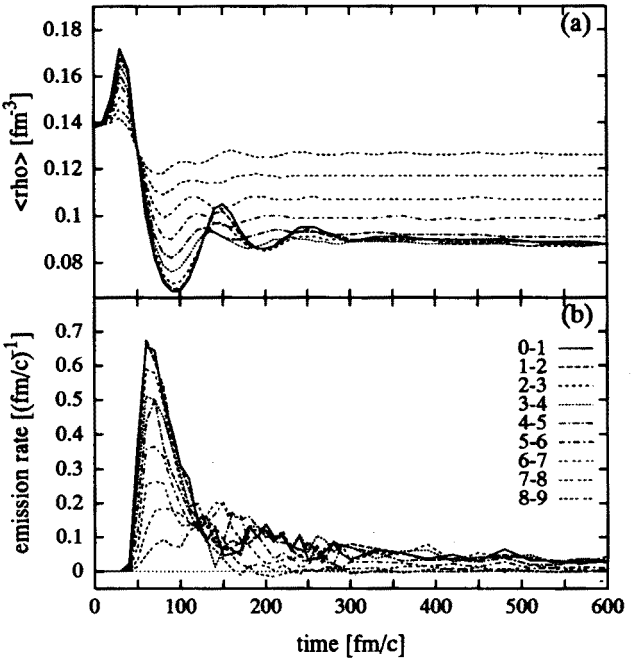

Fig. 4. The time evolution of mean densities (a) and emission rates (b) for various impact parameters. The impact parameter ranges in fm are specified in the legend in the lower part of the figure.

densities and the emission rates are strongly correlated. The fused system is formed in the very early phase of the reaction ($t < 50$ fm/c) and the maximum compression of this system depends on the impact parameter. A dramatic growth of the emission rate is observed after 50 fm/c. The strong variation of average densities and emission rates settle down at a time period shorter than 150 fm/c.

In Fig. 5 we show the temporal evolution of the charge distribution of the ^{84}Kr+^{159}Tb system. Here we observe also fast evolution of the system in the early phase of the reaction, and after 150 fm/c, the shape of the charge distribution changes very slowly.

One of the most interesting questions in this intermediate energy domain of the collision is whether the system reaches global equilibrium. The quantity which allows to investigate this question is the z-th component of the quadrupole moment tensor of the one-body density (Eq. (22)) in the momentum space:

$$Q_{zz} = \frac{\int (3p_z^2 - p^2) g(\vec{p}) d^3p}{\int g(\vec{p}) d^3p}, \tag{22}$$

where the one-body density in momentum space was defined in Eq. (3).

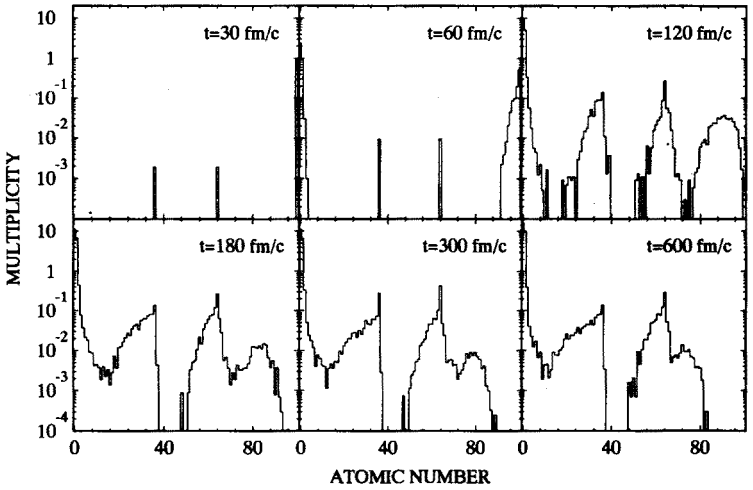

Fig. 5. The time evolution of Z distribution.

The time evolution of the quadrupole moment is shown in Fig. 6. Here, we can clearly see that the system needs about 150 fm/c to equilibrate. We observe also a considerable transverse momentum transfer for more violent collisions.

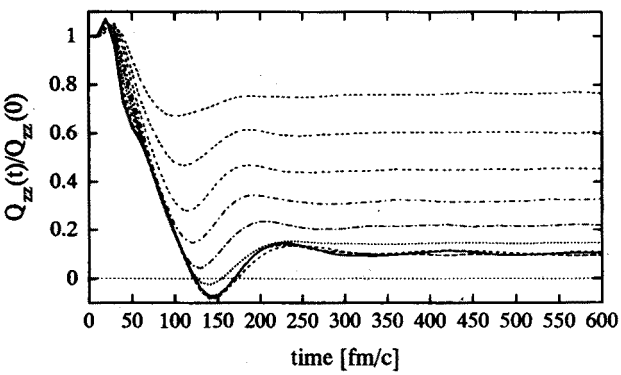

Fig. 6. Time evolution of the relative quadrupole moment in momentum space. The lines correspond to the same impact parameter ranges as in Fig. 4.

The above implies that the time evolution of the reaction at the intermediate energy can be split into two phases. During the first phase within the time interval of the order of 150 fm/c the evolution of the system is dramatic. At the end of this short-time-scale phase the variation of the investigated quantities considerably slows down and becomes smooth. However, a long-time-scale evolution of the reaction may extend up to 10^{-16} s ($3 \cdot 10^7$

fm/c). Such a long lasting process cannot be studied in the framework of this model due to extremely long computer time required and the possible error propagation. We will come back to this question later in this section.

Now, we shall focus on the characteristics of the reaction at the end of the short time scale phase. Thus, we shall stop the dynamical evolution at 300 fm/c.

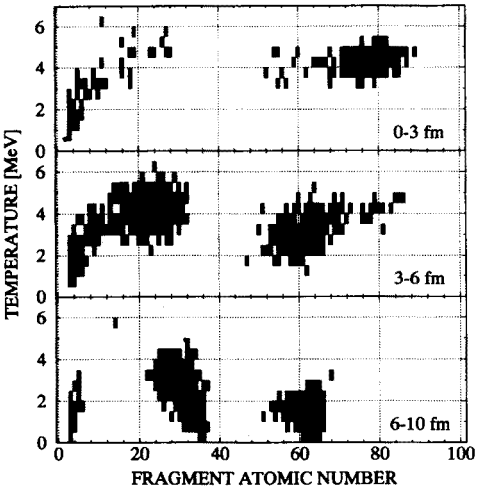

Fig. 7. Temperature vs fragment atomic number.

In Figure 7 we present a scatter plot of the number of events versus fragment charge and temperature (see Eq. (20)) The calculations were performed for three impact parameter regions. We note, that the highest temperature was attained in the fused system and projectile like fragments for the violent collisions. The binary reaction products emerge with different temperatures and the target like fragments are colder than the projectile like fragments. The above calculations show that the fragments are hot at the beginning of the long time scale evolution of the reaction. We already mentioned that highly excited fragments may decay in the time scale of the order $3 \cdot 10^7$ fm/c which is out of scope of this model. In order to study the asymptotic characteristics of the reaction products, we will apply a statistical dynamical code COOLER [26]. These investigations are the subject of another paper [27]. One of the observables which stays unchanged during the long time phase of the evolution of the system is the amount of linear momentum transferred from the projectile to the fused system. This quantity can be obtained either from the fission measurement by looking at the folding angle between two fragments [28], or from the velocity spectrum of the evaporation residues [29]. Systematics of the energy dependence of

the most probable linear momentum transfer in reactions induced by various projectiles was presented by several research groups (see *e.g.* [30]). Fig. 8(a) displays the temporal evolution of the fraction of projectile momentum carried by the fused system ($Z > 71$) and calculated for the central collision ($b \leq 3$ fm).

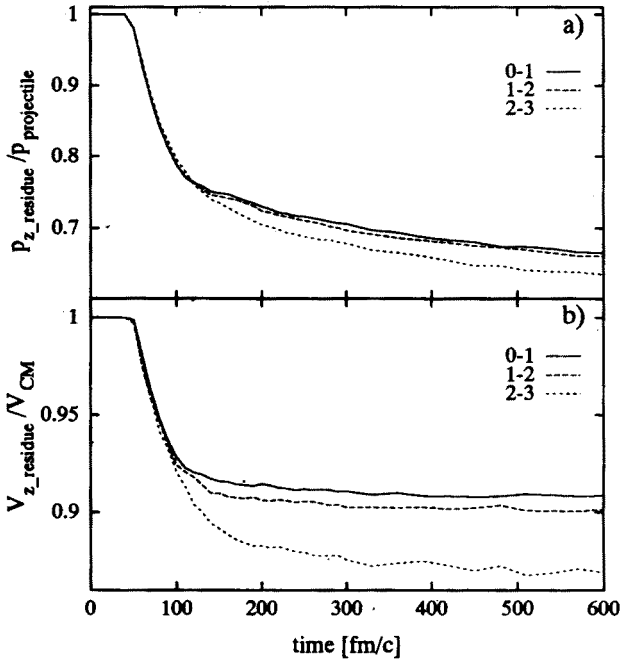

Fig. 8. Linear momentum transfer to the heavy residue (a) and the velocity of this residue in the V_{CM} units (b). The respective lines correspond to the impact parameter ranges in fm, specified in the legends.

During the early phase of the collision ($t < 150$ fm/c) we note a quick decrease of the longitudinal momentum of the composite system. This behaviour is correlated with the high emission rate at the same time interval observed in Fig. 4(b). Since the residue continues to decay after $t = 150$ fm/c its longitudinal momentum decreases slowly. In order to estimate at which moment the preequilibrium emission becomes negligible and the system deexcites statistically we calculated the temporal evolution of the longitudinal velocity of the heavy residue in the laboratory frame. Fig. 8(b) shows that after $t = 150$ fm/c the longitudinal velocity of the residue remains constant. Therefore, we conclude that the composite system produced in the central collision between the Kr projectile and Tb target nucleus at 45 MeV/nucleon attains equilibration in a time shorter than 150 fm/c. After this time interval the longitudinal momentum carried by the heavy residue

is about 75 percent of the projectile momentum. This value agrees with the experimental systematics of the most probable momentum transfer [30].

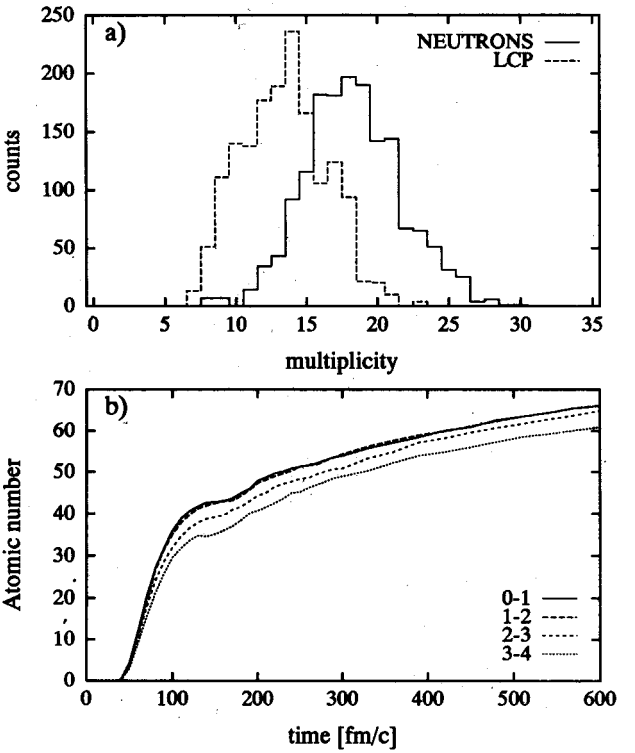

Fig. 9. Neutron and LCP multiplicities at 150 fm/c for the central collisions (a) and the time evolution of the mass of light fragments emitted (b). The lines in part (b) of the figure correspond to the impact parameter ranges in fm, specified in the legend.

Model calculations allow also to distinguish different modes of preequilibrium emission. Fig. 9(a) displays the multiplicity distributions for the neutrons and light charged particles emitted in the early phase of the reaction ($t = 150$ fm/c) calculated for the central collision ($b < 4$ fm). Fig. 9(b) shows that the total emitted mass in the preequilibrium stage is about a half of the projectile.

Combining this result with the earlier estimated value of the linear momentum transfer we conclude that the most common assumption describing nonequilibrium nucleons as emitted with a beam velocity leads to the overestimation of the composite system mass.

4. Conclusions

We have presented a microscopic dynamical model of heavy ion collision at intermediate energies which is particularly useful to study the early phase of the reaction. This approach makes possible to follow the time evolution of the N-body system from the initial configuration to the final distribution of nucleons on an event-by-event basis. We have applied the model to simulate the reaction $^{84}Kr+^{159}Tb$ reaction at 45 MeV/nucleon which has been studied experimentally.

The investigation of the temporal evolution of the z-th component of the quadrupole moment tensor of the one body density in the momentum space leads to the conclusion that the system needs about 150 fm/c to equilibrate. This observation and the calculations of the time evolution of the mean density and emission rate imply that the reaction between heavy ions can be split into two phases. The first phase of the order of 150 fm/c characterized by dramatic changes of the system. During the second phase which may extend up to $3 \cdot 10^7$ fm/c the evolution of the system slows down.

We calculated also the amount of linear momentum transferred from the projectile to the fused system which is produced for the central collision ($b < 3$ fm). This quantity fits to the experimental systematics of the most probable momentum transfer.

Further studies concerning fragment production and the nuclear equation of state are in progress.

We wish to thank Dr. J. Aichelin for providing us three routines which we found useful during the code preparation. We are also obliged to Dr. R.P. Schmitt for reading the manuscript and valuable comments.

The calculations were performed on SUN 670 MP at Jagellonian University Computer Centre and on CONVEX C3200 at Academic Computer Centre CYFRONET.

REFERENCES

[1] P. Siemens, *Nucl. Phys.* **A428**, 189c (1984).

[2] P. Bonche, S.E. Koonin, J.W Negele, *Phys. Rev.* **C13**, 1226 (1976); S.E. Koonin, *et al.*, *Phys. Rev.* **C15**, 1359 (1977); D. Vautherin, J. Treiner, M. Vénéroni, *Phys. Lett.* **B191**, 6 (1987); K.T.R. Davies, S.E. Koonin, *Phys. Rev.* **C23**, 2042 (1981).

[3] Y. Yariv, Z. Fraenkel, *Phys. Rev.* **C20**, 2227 (1979); J. Cugnon, *Phys. Rev.* **C22**, 1885 (1980); J. Cugnon, T. Mizutani, J. Vandermeulen, *Nucl. Phys.* **A352**, 505 (1981); J. Cugnon, *Nucl. Phys.* **A387**, 191c (1982).

[4] J.P. Bondorf, *Nucl. Phys.* **A387**, 25c (1982); W. Lynch, *Ann. Rev. Nucl. Part. Sci.* **37**, 493 (1987); D.H.E. Gross, *Rep. Prog. Phys.* **53**, 605 (1990).

[5] M. Gyulassy, K.A. Frankel, H.Stöcker, *Phys. Lett.* **110B**, 185 (1982); P. Danielewicz, G. Odyniec, *Phys. Lett.* **157B**, 146 (1985); H.H. Gutbrod, A.M. Poskanzer, H.G. Ritter, *Rep. Prog. Phys.* **52**, 1267 (1989); J. Péter, *et al.*, *Nucl. Phys.* **A519**, 127c (1990).

[6] C.Y. Wong, T. Welton, *Phys. Lett.* **49B**, 243 (1974); C.Y. Wong, J.A. McDonald, *Phys. Rev.* **C16**, 1196 (1977); J.R. Nix, *Prog. Part. Nucl. Phys.* **2**, 237 (1979).

[7] E.A. Uehling, G.E. Uhlenbeck, *Phys. Rev.* **43**, 552 (1933); G.F. Bertsch, H. Kruse, S. Das Gupta, *Phys. Rev.* **C29**, 673 (1984); J. Aichelin, G.F. Bertsch, *Phys. Rev.* **C31**, 1730 (1985); H. Kruse, *et al.*, *Phys. Rev.* **C31**, 1770 (1985).

[8] J. Aichelin, H. Stöcker, *Phys. Lett.* **176B**, 14 (1986); G. Peilert, *et al.*, *Phys. Rev.* **C39**, 1402 (1989); G. Peilert, *et al.*, *Nuclear Dynamics and Nuclear Disassembly*, ed. J.B. Natowitz, Proc. of the Symposium, World Scientific, Dallas, Texas, Apr. 1989; A. Bohnet, *et al.*, *Nucl. Phys.* **A494**, 349 (1989); C. Hartnack, *et al.*, *Nucl. Phys.* **A495**, 303c (1989); L. Neise, *et al.*, *Nucl. Phys.* **A519**, 375c (1990); T. Maruyama, *et al.*, *Nucl. Phys.* **A534**, 720 (1991); A. Bohnet, *et al.*, *Phys. Rev.* **C44**, 2111 (1991); P. Valta, *et al.*, *Nucl. Phys.* **A538**, 417c (1992); G. Peilert, *et al.*, *Phys. Rev.* **C46**, 1457 (1992); W. Müller, M. Begemann-Blaich, J. Aichelin, *Phys. Lett.* **298B**, 27 (1993).

[9] J. Aichelin, *et al.*, *Phys. Rev.* **C37**, 2451 (1988).

[10] J. Aichelin, *Phys. Rep.* **202**, 233 (1991).

[11] D.H. Boal, J.N. Glosli, *Phys. Rev.* **C38**, 1870 (1988).

[12] D.H. Boal, J.N. Glosli, *Phys. Rev.* **C38**, 2621 (1988); D.H. Boal, J.N. Glosli, C. Wicentowich, *Phys. Rev.* **C40**, 601 (1989); D.H. Boal, J.C.K. Wong, *Phys. Rev.* **C41**, 118 (1990).

[13] E. Wigner, *Phys. Rev.* **40**, 749 (1932); P. Carruthers, F. Zachariasen, *Rev. Mod. Phys.* **55**, 245 (1983); M. Hillery, *et al.*, *Phys. Rep.* **106**, 121 (1984).

[14] S.R. de Groot, L.G. Suttorp, *Foundations of Electrodynamics*, North-Holland Publ. Co., Amsterdam 1972, chapt. VII.

[15] C. Cariano, R. Parwani, H. Yamagishi *Nucl. Phys.* **A552**, 591 (1991).

[16] M.A. Preston, R.K. Bhaduri, *Structure of the Nucleus*, Addison-Wesley Pub. Co., Reading, Massachusetts 1975, p. 306.

[17] L. Wilets, *et al.*, *Nucl. Phys.* **A282**, 341 (1977); L. Wilets, Y. Yariv, R. Chestnut, *Nucl. Phys.* **A301**, 359 (1978); D.J.E. Callaway, L. Wilets, Y. Yariv, *Nucl. Phys.* **A327**, 250 (1979).

[18] C. Dorso, S. Duarte, J. Randrup, *Phys. Lett.* **188B**, 287 (1987); C. Dorso, J. Randrup, *Phys. Lett.* **215B**, 611 (1988); C. Dorso, J. Randrup, *Phys. Lett.* **232B**, 29 (1989).

[19] H. Horiuchi, A. Ohnishi, T. Maruyama, Proc. of the 6-th International Conference on Nuclear Reaction Mechanisms, Varenna, June 10-15, 1991, ed. E. Gadioli.

[20] N. Metropolis, *et al.*, *J. Chem. Phys.* **21**, 1087 (1953).

[21] G. Peilert, *et al.*, *Phys. Lett.* **260B**, 271 (1991).

[22] T. Maruyama, A. Ohnishi, H. Horiuchi, *Phys. Rev.* **C42**, 386 (1990).

[23] G.F. Bertsch, S. Das Gupta, *Phys. Rep.* **160**, 189 (1988).
[24] K. Huang, *Statistical Mechanics,* John Wiley and Sons, Inc., New York 1963, p. 150.
[25] Z. Majka, *et al.*, in the Proceedings of the Symposium on Nuclear Dynamics and Nuclear Disassembly, World Scientific, ed. J.B. Natowitz, Dallas 1989, p.424.
[26] T. Kozik, to be published.
[27] J. Łukasik, to be published.
[28] T. Sikkeland, E.L. Haines, V.E. Viola Jr., *Phys. Rev.* **125**, 1350 (1962); B.B. Back, *et al.*, *Phys. Rev.* **C22**, 1927 (1980); M.B. Tsang, *et al.*, *Phys. Lett.* **134B**, 169 (1984).
[29] V.E. Viola, *et al.*, *Phys. Rev.* **C26**, 187 (1982).
[30] J. Jastrzębski, *et al.*, *Phys. Lett.* **136B**, 153 (1984); S. Leray, *J. Phys.* **47**, C4-275 (1986).